Hexaquarks at CLAS12

M.Bashkanov, G. Clash, M. Nicol, D.P. Watts, N. Zachariou

December 2019

Abstract

Recently discovered $d^*(2380)$ hexaquark is expected to be the first particle from a SU(3) hexaquark antidecuplet. A search for heavy strange partners of the $d^*(2380)$ is a challenging task. In this analysis note we propose strategies we plan to exploit in our studies of this hexaquark antidecuplet. Most promising hexaquark candidates with strangeness zero, one, two, and three are identified and will be studied based on CLAS12 run group B data by the York group. Several PhD students are allocated for these studies.

1 Introduction

Quantum Chromo Dynamics (QCD) is responsible for the binding of quarks into hadrons. In recent years plenty of new states in four-, five-, and six-quark sectors were discovered [1, 2, 3, 4, 5]. Some of them were properly identified as loosely bound molecular states. For many others, the internal structure is not known, which raises a question of many-body effects in QCD, as well as the interplay between genuine multiquarks and molecular states. To properly study the internal structure of a composite state, large production rates together with the ability to cleanly select events are required. This essentially rules out the detailed study of states with heavy quarks, since these cannot be produced in large quantities at the current experimental facilities. From another hand, four-and five-quark states made of only light quarks cannot be reliably disentangled from conventional states. That makes 6q states a natural choice to study multiquark systems in vitro. Out of several 6q states we know, the $d^*(2380)$ with $J^P = 3^+$ is the most promising candidate: it is located far from any thresholds, and hence the 6q component - as opposed to the molecular one - is expected to be very large [3, 4, 5, 6, 7, 8, 9, 10, 11]. Theory studies also predict large hexaquark components for this state [12, 13]. Several opportunities are accessible to us in attacking the multiquark structure of 6q states.

1.1 Astrophysical implications of Hexaquarks

The role of a $d^*(2380)$ degree of freedom for the nuclear equation of state, EoS ([14]) was recently studied in several papers [15, 16]. The $d^*(2380)$ is a massive positively charged non-strange particle with integer spin (J=3) and it is the first predicted non-trivial hexaquark supported by experiment ([4, 5, 6]). The importance of such a new degree of freedom resides in the fact that it has the same u, d quark composition as neutrons and protons and, therefore, does not involve any strangeness degrees of freedom. Moreover, it is a boson and as such, can condense within neutron stars. It was shown that despite its large mass, the $d^*(2380)$ can appear in the neutron star (NS) interior at densities similar to those predicted for the appearance of other proposed states e.g. nucleon resonances, Δ's, or hyperons. The effect of the $d^*(2380)$ on the nuclear equation of state (EoS) was studied both in non-interacting and interacting cases (both attractive and repulsive). The results indicate the $d^*(2380)$ has the potential to be an important new degree of freedom in neutron stars. Fractions of $d^*(2380)$ of around 20% are predicted in the centre of heavy stars, resulting in an increased maximum star radius and a reduced central density. New neutrino and antineutrino cooling mechanisms are possible with $d^*(2380)$ formation, which have previously not been included in neutron star modelling. The EoS with explicit $d^*(2380)$ degrees of freedom is one of the few which predict NS mass-radius relation consistent with the latest (subsequent) gravitational wave experimental results [17]. Indeed, the presence of the $d^*(2380)$ is predicted to set a strict limit on a maximum neutron star mass in agreement with that inferred from gravitational wave data [15, 16]. As an isoscalar particle, the interaction of the d^* is reduced to isoscalar (dominantly σ, ω) exchanges. Interplay between the $d^*(2380)$ dimensionless coupling constants ($x_{\sigma d^*} = \frac{g_{\sigma d^*}}{g}$, $x_{\omega d^*} = \frac{g_{\omega d^*}}{g_{\omega N}}$) and its chemical potential in neutron star matter are shown on Fig. 1. As

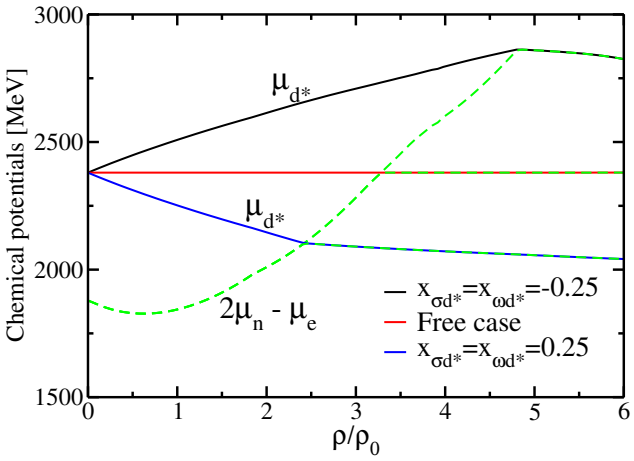

Figure 1: Chemical equilibrium condition for the appearance of the $d^*(2380)$ hexaquark in β-stable matter. Results are shown for the cases in which the $d^*(2380)$ feels attraction ($x_{\sigma d^*} = x_{\omega d^*} = 0.25$), repulsion ($x_{\sigma d^*} = x_{\omega d^*} = -0.25$) or does not interact at all with the rest of the particles of the system.

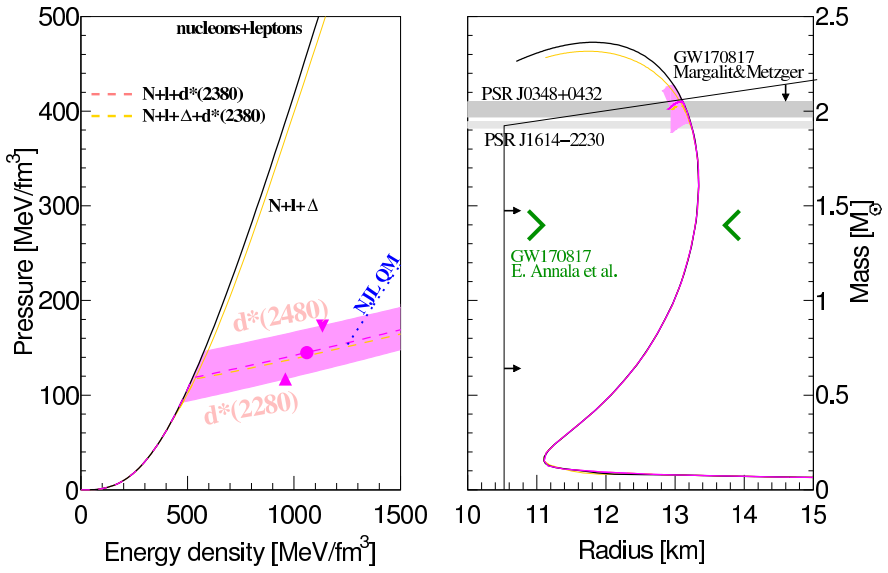

Figure 2: Neutron star EoS (left) and mass-radius relation (right) with and without the d^* degree of freedom. The predictions assuming $m_{d^*} = [2280, 2480]$ MeV and $m_{d^*} \equiv 2380$ MeV are shown by the shaded bands and dashed pink lines respectively. The effect of the Δ degree of freedom is shown as a gold line with $d^*(2380)$(dashed) and without (solid). The observational masses of the pulsars PSR J1614-2230 ($1.928 \pm 0.017 M_\odot$) [18] and PSR J0340+0432 ($2.01 \pm 0.04 M_\odot$) [19] as well as neutron star merger GW170817 limits from [17] and [20] are also shown. The pink markers on a left panel represent the maximum achievable pressure/energy density for heavy neutron star with d^* degrees of freedom for the $m_{d^*} = 2380$ MeV(circle), 2280 MeV and 2480 MeV(triangles). Pure NJL quark matter EoS is shown by dashed blue line.

expected, an attractive interaction between the d^*'s and the nuclear matter leads to the earlier appearance of the d^* (in terms of nuclear density) in nuclear matter and a stronger reduction of the fractional protons and neutron composition [16]. The EoS and corresponding NS mass-radius relation in presence of the d^* can be seen on Fig. 2.

Furthermore, it was recently indicated that the Bose-Einstein condensates of the d^*-hexaquarks could

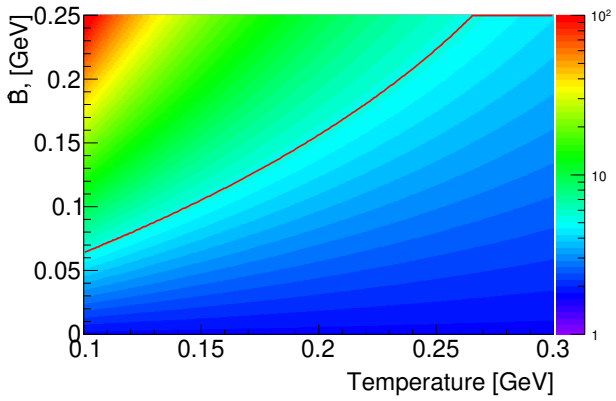

Figure 3: The primordial production of $d^*(2380)$-BEC (expressed as a ratio to baryon matter) calculated as a function of binding energy per baryon, $\hat{B}$ and matter-dark matter decoupling temperature. The red line shows the loci corresponding to the current experimental determination of the dark matter to matter ratio[**?**].

be produced copiously in the early universe and might contribute to dark matter, Fig. 3, see Ref. [21] for details. From these, it is clear that the extraction of the d^*'s properties, such as its size, structure, magnetic moment, and quadrupole deformation have a strong potential impact for astrophysics as well as for hadron and strong interaction physics. The properties of heavy d^* SU(3) multiplet members constrain the d^*'s structure (molecular vs hexaquark) as well as contribute to a "hyperon puzzle" problem and cooling of the early Universe.

2 $d^*(2380)$ multiplet

As any strongly interacting particle, the $d^*(2380)$ appears as an SU(3) multiplet member. Specifically, in the case of the $d^*(2380)$, it would be antidecuplet, as shown in Fig. 4. Spectroscopic study of other multiplet members can shed light on the d^*'s internal structure, complimentary to Form-Factor studies. In the molecular picture, the d^* SU(3) multiplet appears as a molecule made of two baryon decuplet members: from $\Delta\Delta$ for the $d^*(2380)$ to $\Delta\Omega$ for the d_{sss}, bound by a long-range pion exchange. However, since pion does not couple to strange quarks, the binding energy in molecules should decrease with an increase of strangeness content. In a hexaquark picture, the increase of mass driven by heavier s-quarks would imply stronger binding for the strange members. That is why we propose this measurement that will allow the discovery of all d^* multiplet members. This study will allow us to constrain 6q dynamics of multiquark systems.

Generally, all d^*-multiplet members can decay into two baryon decuplet states or two baryon-octet states. The $d^*(2380)$ decays predominantly into two decuplet baryons – $\Delta\Delta$. Although two octet baryons have much larger phase space, the decay branch $Br(d^* \to pn) \sim 10\%$. The same is expected for all multiplet members, hence all decays would have large multiplicity final states.

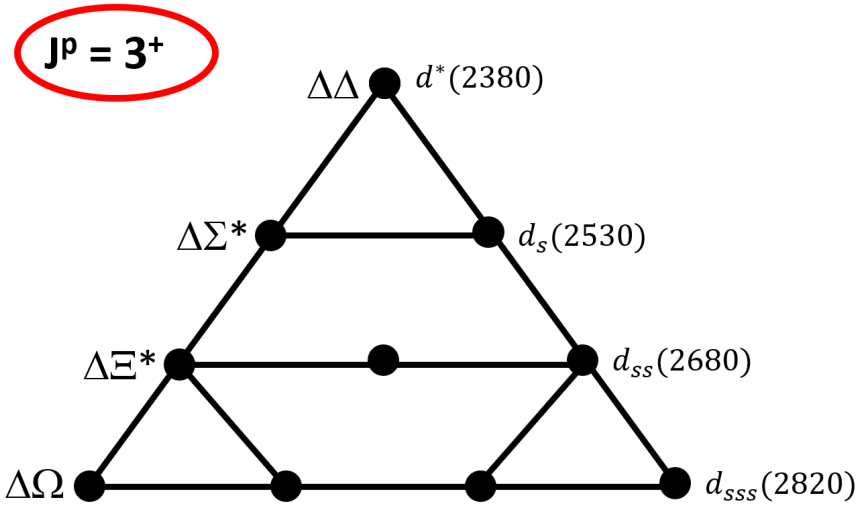

Figure 4: $d^*(2380)$ multiplet

3 $d^*(2380)$ photo and electroprduction.

The d^* electroproduction is the ultimate method to extract the internal properties of the d^*. Similar studies were recently performed with various N^* resonances, where the measurement of transition form factor allowed for greater understanding of their nature (e.g. prove the molecular properties of the Roper resonance, $N^*(1440)$). In the vast majority of electroproduction reactions, single photon exchange is the dominant process and two-photon exchange processes can be completely neglected. Unfortunately, this is not the case for the $d^*(2380)$, where the $d^* \to d\gamma\gamma$ transition is larger than $d^* \to d\gamma$. The majority - about 90% -of the d^* decay branches proceed via $d^* \to \Delta\Delta$ [11], in particular $Br(d^* \to \Delta\Delta \to d\pi\pi) \sim 37\%$. The photon decay of a Δ resonance is also large $Br(\Delta \to N\gamma) \sim 0.6\%$ or 0.7 MeV. Assuming these branching fractions and a total width of the $\Gamma(d^*) \approx 80$ MeV, one can estimate $\Gamma(d^* \to d\gamma\gamma) \approx 1.2$ keV. Similarly, one can evaluate the $\Gamma(d^* \to d\gamma)$ from A2 and ELPH measurements of the d^* photoproduction cross-section $\sigma(\gamma d \to d^* \to d\pi^0\pi^0) = 28nb$ [22, 23]. Accounting for a $Br(d^* \to d\pi^0\pi^0) = 14\%$, one will get $\sigma(\gamma d \to d^*) \sim 200\ nb$ or $\Gamma(d^* \to d\gamma) \sim 0.6\ keV$. Such an unusually large ratio between double and single photon branches might lead to strong interference effects in d^*-electroproduction making the experiment more sensitive to exotic degrees of freedom. However, it also requires better knowledge of the single photon branch. Fortunately, such studies can be performed with an independent experiment with a real photon beam.

3.1 d^* photoproduction

With deuteron quantum numbers of $J^p = 1^+$ and the d^* being $J^p = 3^+$, there are only three possible multipolarities which can be involved in $\gamma d \to d^*$: $E2, M3$ and $E4$. On a quark level, that would correspond to a spin-flip of 2,3 and 4 quarks respectively [1]. These transitions are proportional to the electric transition quadrupole moment, $Q_{d\to d^*}$, to the magnetic transition octupole moment, $\Omega_{d\to d^*}$, and to the electric transition hexadecapole moment $D_{d\to d^*}$, respectively [24]. The $E4$ transition is expected to be highly suppressed, and therefore we assume in all subsequent chapters that only $E2$ and $M3$ transitions contribute (unless otherwise explicitly stated). There are two and only two channels where the d^* can be observed in photo-/electro- production: $d^* \to d\pi^0\pi^0$ and $d^* \to pn$. In the latter, a partial wave decomposition is essential. In any other channels, including $d^* \to d\pi^+\pi^-$, the level of conventional background exceeds the d^* signal by 2-3 orders of magnitude making any reliable analysis challenging. Both $d^* \to d\pi^0\pi^0$ and $d^* \to pn$ channels were analysed intensively with the Crystal Ball, at MAMI Mainz. Details can be found in Refs. [25, 26]. An exploratory analysis is foreseen for the $d^* \to d\pi^0\pi^0$ channel Fig.5, while deuteron electrodisintegration reaction is a standard calibration process for many run groups, no further simulation studies are necessary.

It was recently shown [27] that one can access the NN^* Final State Interaction (FSI) in $\gamma d \to d\pi^0\pi^0$. While the data of Ref.[27] was not very conclusive, such a possibility requires an independent check.

As a starting point, we have simulated Phase Space $ed \to e'd\pi^0\pi^0$ weighted with $1/q^2$ dependence for the virtual photon, Fig.5. The expected acceptance is fairly low, however, in the case of one or two π^0 detection, the energy dependence of acceptance is fairly smooth and rather flat which ensure the absence of acceptance related bump production. The expected statistics is rather low. We expect a few thousand reconstructed events up to the 3rd resonance region. An exploratory analysis should be sufficient to identify possible issues with this channel.

[1] Generally one would expect that higher multipoles should be suppressed and that the main transition amplitude should be $E2$. In a similar case of $N \to \Delta$ transition, the main multipole is $M1$ with $E2$ being of a few per cent only.

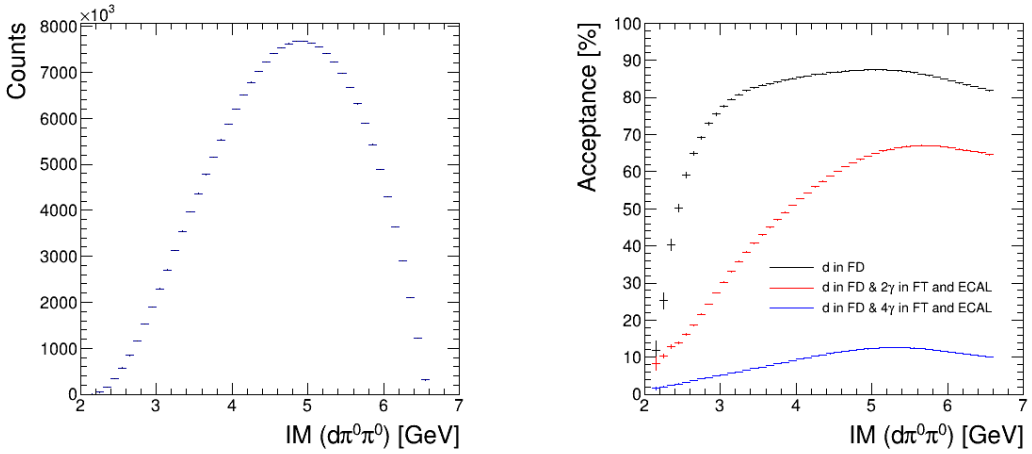

Figure 5: Simulated $d\pi^0\pi^0$ invariant mass(left) and reaction acceptance as a function of $M_{d\pi\pi}$ (right). Phase space MC with $1/q^2$ weight for a virtual photon. Black line correspond to acceptance of the reaction if only deuteron are measured in FD; red: d in FD and 2 photons in FT/ECAL; blue: d in FD, 4 photons in FT/ECAL

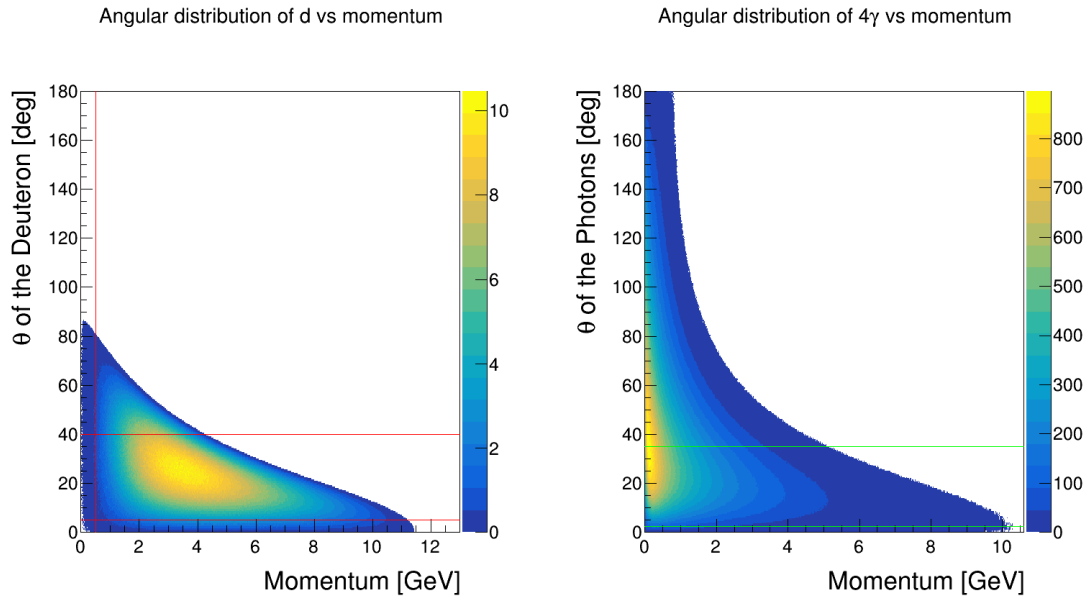

Figure 6: Simulated angular distributions for the $\gamma^* d \to d\pi^0\pi^0$ events

4 d_s -state

There was a preliminary d_s search performed based on CLAS6 g13 data, attempting to study $d_s \to \Sigma^* \Delta$ decay $d_s \to \Sigma^{*-}\Delta^{++} \to \Lambda\pi^- p\pi^+ \to 2\pi^- 2p\pi^+$. To conserve strangeness, a d_s production needs to be accompanied by a kaon. With two charge states of d_s^+ and d_s^0, it could be both K^+ and K^0, however, to suppress diagrams with kaon in flight production(Fig 22), contributing largely to a background reactions we concentrate on a process with neutral kaon in a final state: $\gamma d \to K^0 d_s$. A typical diagram leading to production of the d_s is shown on Fig. 7.

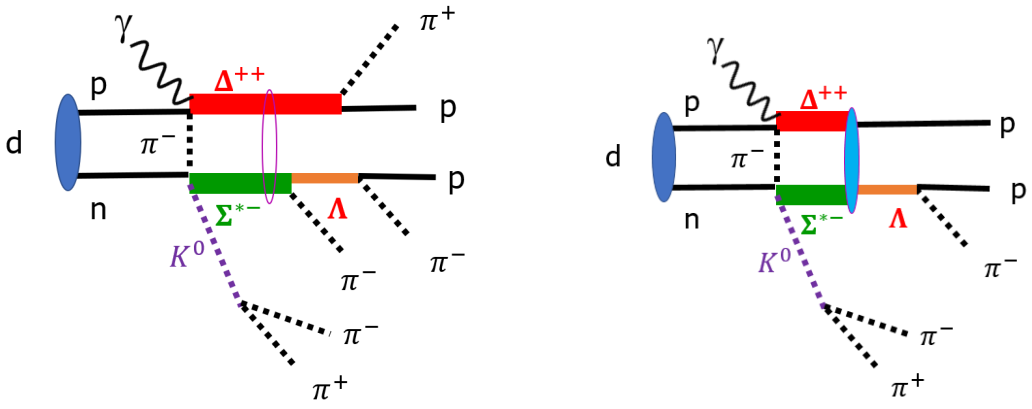

Figure 7: d_s photoproduction graph with decay to Decuplet+Decuplet (left) and Octet+Octet (right).

A very high-multiplicity final state for the reaction $\gamma d \to K^0 d_s \to 3\pi^- 2\pi^+ 2p$ reduces detection efficiency substantially; however, as a byproduct, it strongly increases the purity of the selected process. Fig 8 shows the main steps of event selection. The resulting distribution shows pretty clean $\Sigma^* \Delta$ spectrum, which agrees

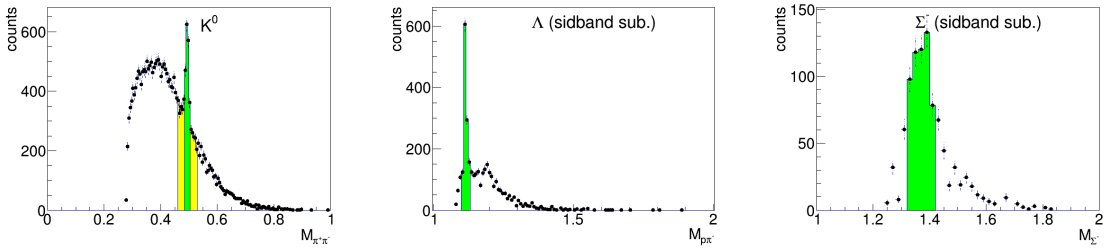

Figure 8: d_s selection steps. Left panel: K^0 selection from $\pi^+\pi^-$ signal(green) and sidebands(yellow). Middle Panel: Λ selection from $p\pi^-$. Right Panel: Σ^* selection from $\Lambda\pi^-$

very well with simulations with possible but insignificant enhancement at d_s mass, Fig. 9.

Generally speaking, it should be sufficient to measure only the K^0, observing d_s in a missing mass spectrum. To increase statistics, we consider restricting ourselves to the detection of K^0 to extract the missing mass and two protons to ensure the two-nucleon dynamics of the reaction. This way also the elastic channel $d_s \to \Lambda p$ can be partially accessed. We do not expect to see any signal in the Λp channel unless the polarisation observables based on Λ recoil polarisation are involved, similarly to the $d^* \to p\vec{n}$ case. A detailed simulation study of angular distributions and efficiencies can be seen in Fig 10 and Fig 11. The acceptance is smooth and rather large for such a many-body final state.

We expect much larger d_s unrelated backgrounds in K^+ associated reactions. However, this does not exclude $\gamma^* d \to K^+ d_s^0$ from our shopping list, especially in polarisation observables. Indeed, both decay branches $d_s^0 \to n\Lambda$ and $d_s^+ \to p\Lambda$ should lead to 100% polarisation of both nucleons and Λs due to ${}^3D_3$ decay partial wave, but any single nucleon channel hyperon production does not need to have the same polarisation properties due to different photon-nucleon coupling for proton/neutron and due to difference in magnetic

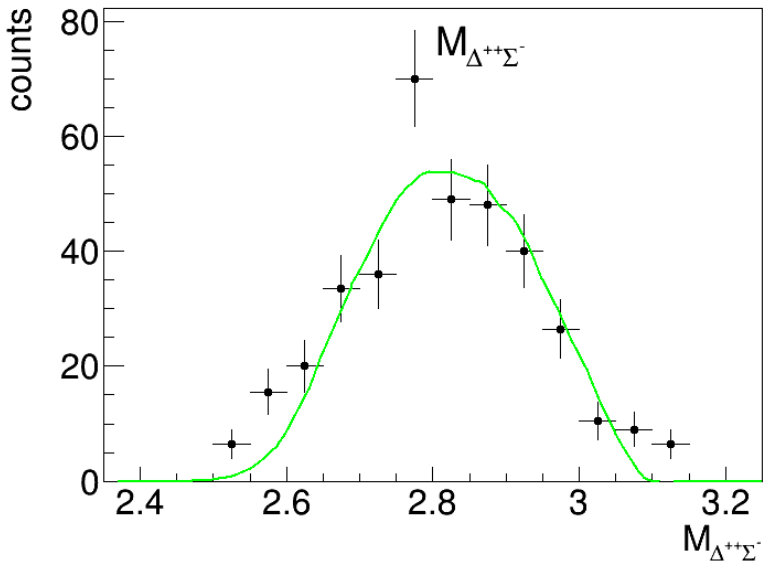

Figure 9: $\Sigma^*\Delta$ spectrum

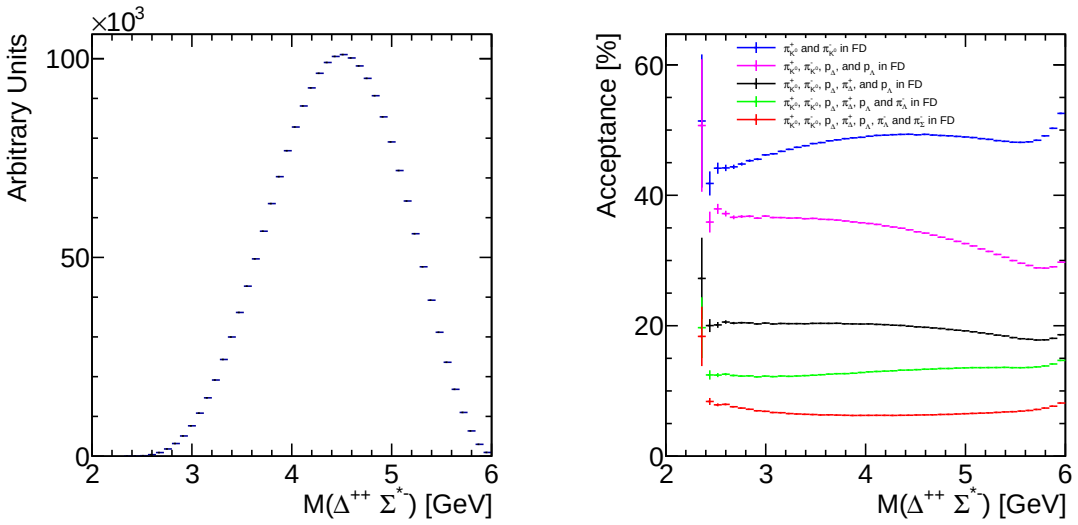

Figure 10: Simulated $\Delta\Sigma^*$ invariant mass(left) and reaction acceptance as a function of $M_{\Delta\Sigma^*}$ (right). (Phase Space MC with $1/q^2$ weight for a virtual photon.). Blue line correspond to acceptance of the reaction if only K^0 are measured in FD; pink: K^0 and 2 protons in FD; black: K^0, 2 proton and π^+ in FD; green: K^0, Δ and in FD; red: K^0, Δ and Σ in FD.

moments of protons/neutrons/N^*'s. That is why a comparison of $n\vec{\Lambda}$ and $p\vec{\Lambda}$ channels can be used for a better background understanding in these channels.

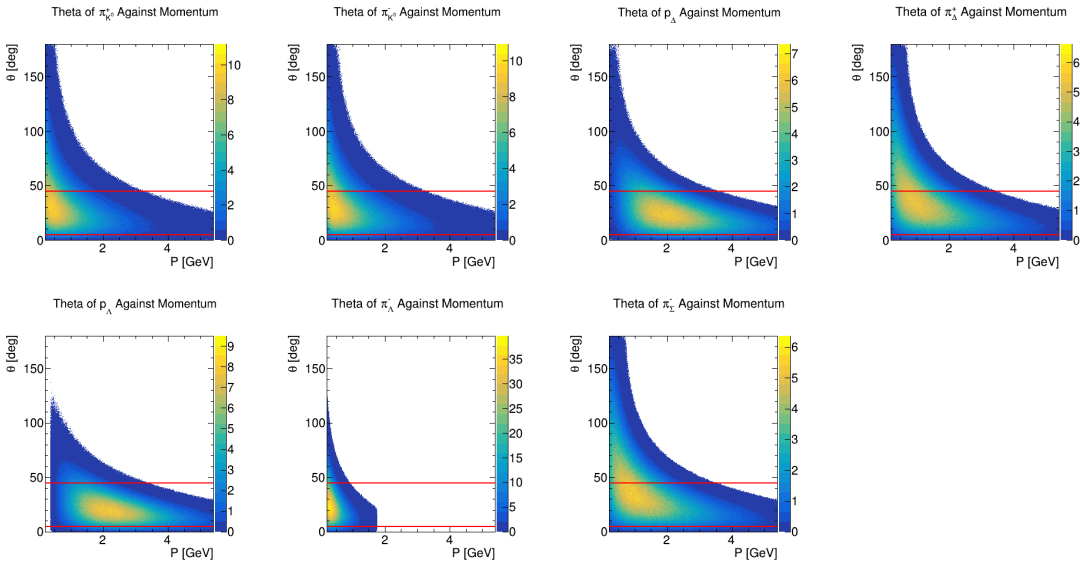

Figure 11: Simulated momentum-angular relations for the $\Delta\Sigma^*$ electroproduction reaction. Horizontal lines highlight the FD acceptance range.(Phase Space MC with $1/q^2$ weight for a virtual photon.)

5 d_{ss}-state

The d_{ss} state appears as an isotriplet with charges from -1 to +1. The most convenient state to search for appeared to be d_{ss}^{-}, since it is accompanied by two K^+ with fairly high detection efficiency and selection purity with positively charged outbending magnetic field. The main background processes originate from Ξ^{*-} production on proton and can be fairly well eliminated by comparison of $\gamma p \to K^+K^+X$ and $\gamma d \to K^+K^+X$ reactions. To increase the purity of the sample and ensure the two-nucleon origin of the reaction, we plan to require both the protons to be detected as part of our selection criteria. The main physical background

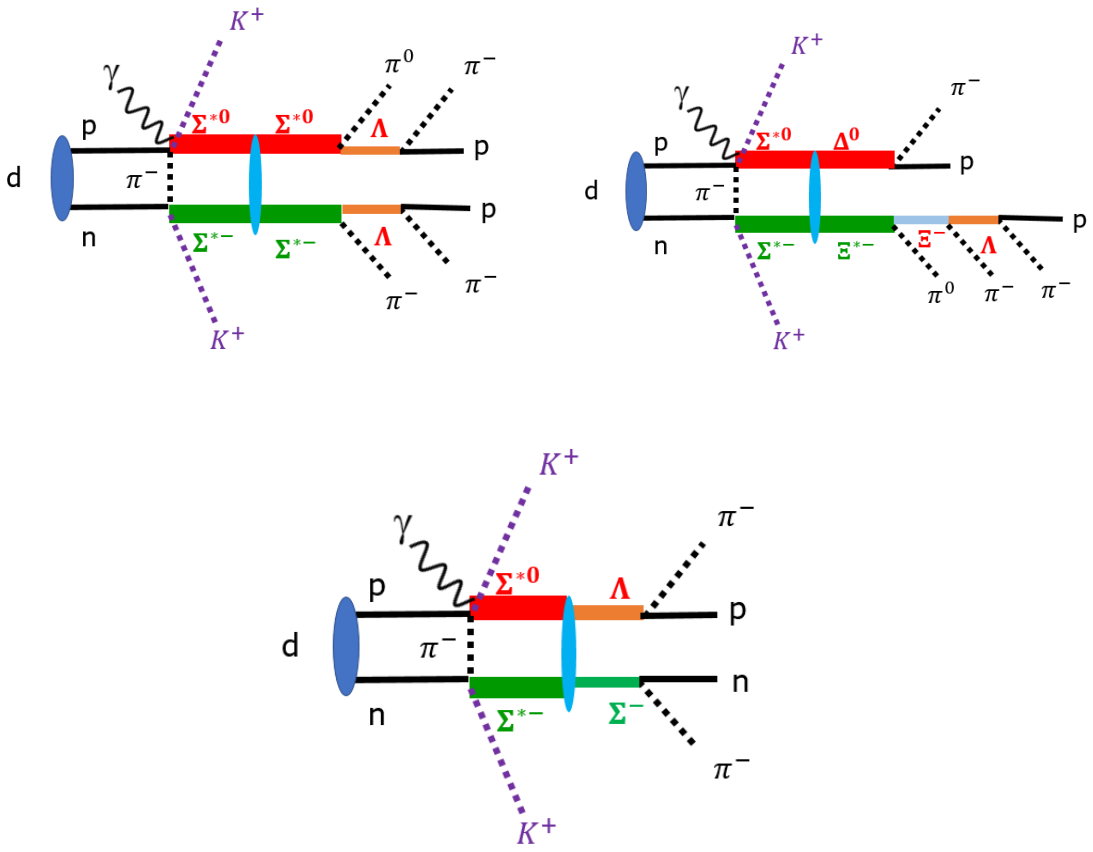

Figure 12: d_{ss} photoproduction graph with $10 \oplus 10$ decay(top row) and $8 \oplus 8$ decay (bottom).

originates from Ξ^{*-} production on proton, however, it is worth noting that neither of the known Ξ^{*-} states can build up a peak in the vicinity of d_{ss} mass, see Fig 13. Here we assumed the same suppression factor for the d_{ss} relative to conventional resonances as for the d^* relative to N^*/Δ's ($\sim$ 100 suppression). For simplicity, all known Ξ's are shown with the same strength. As one can see, the d_{ss} is expected to appear in the region where no Ξ contributes. If we assume a quasi-free K^+K^+ production on proton, Fig 13, the d_{ss} should appear at $M_{d_{ss}} - M_n$.

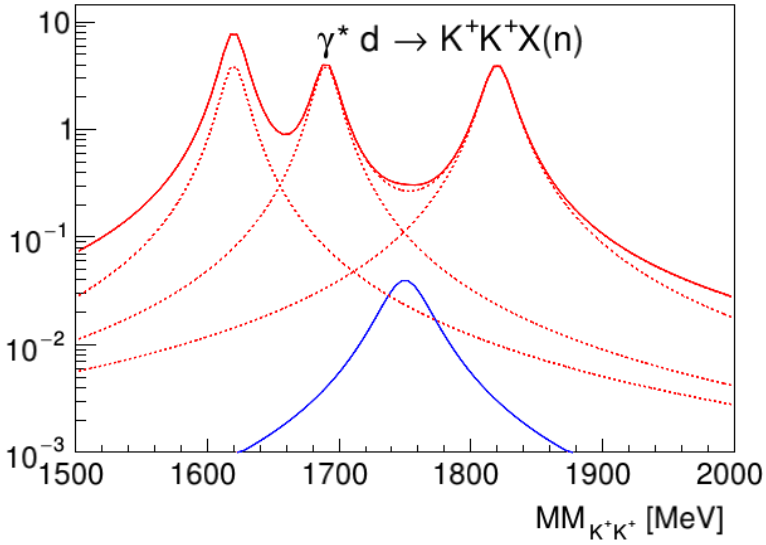

Figure 13: Conventional background in d_{ss} production for the reaction $\gamma d \to K^+K^+X$ without requirement on nucleons in the final state, under assumption of proton target (quasi-free process). Red lines correspond to known Ξ^* states, blue line represent d_{ss}.

6 d_{sss}-state

The d_{sss} state is an ultimate goal of the d^*-multiplet searches. It has isospin $I = 3/2$ and is represented by 4 charge states from $q = -2$ to $q = +1$. The double negative member of the isoquartet appeared to be the most promising one in terms of conventional background. Indeed, conventional background in a $\gamma p \to 3K^+X$ channel is strictly prohibited: to conserve both charge and strangeness, the state X should have charge $q = -2$ and strangeness $s = -3$ which is impossible for a 3q state - the most negative and the only state with strangeness $s = -3$ is the Ω baryon, which has charge $q = -1$. For further discussion about possible nucleon based background for the d^{--}_{sss}, see section 7. The reaction we are looking for in the case of d^{--}_{sss} production can be seen of Fig. 14. A series of simulations were performed to understand the

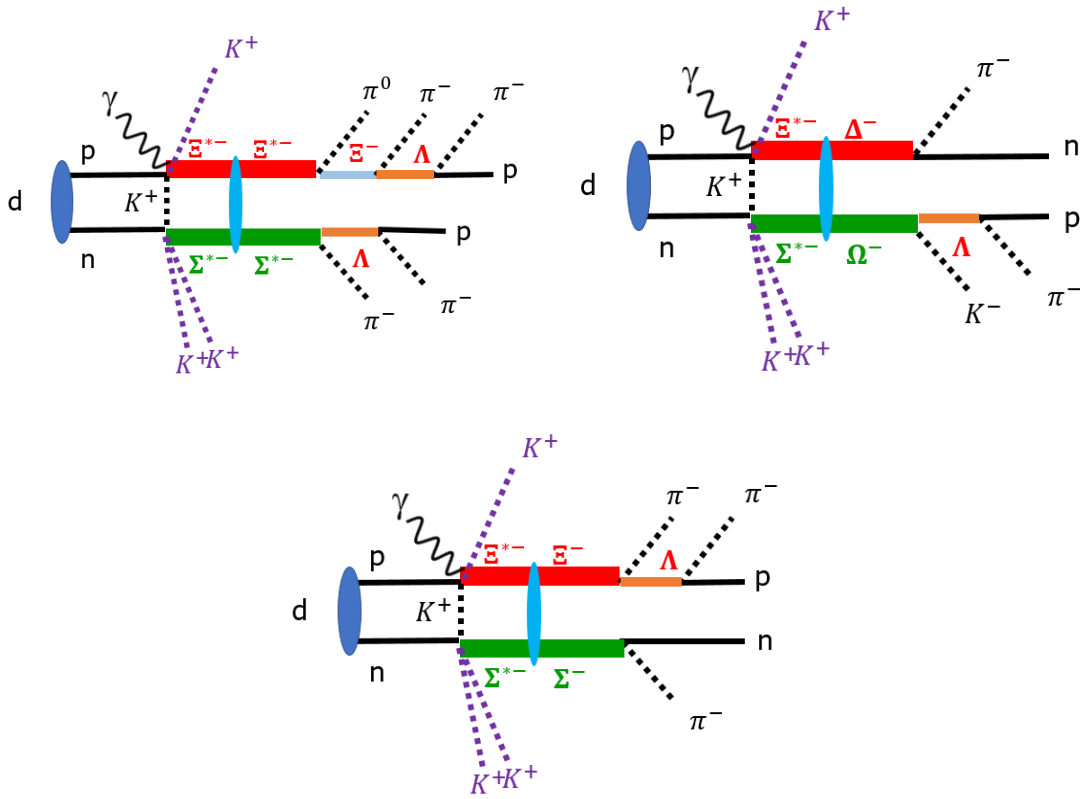

Figure 14: d^{--}_{sss} photoproduction graphs for the Decuplet-Decuplet decay (top row) and Octet-Octed decay bottom.

kinematics of possible d^{--}_{sss} production. It appeared to be that the angular distribution of all three K^+ is favourable to be detected with CLAS12 forward detector, the efficiency is very smooth: no sharp changes in efficiency are found, see Fig. 15. Several reaction decay branches are possible to investigate here, both in $d_{sss} \to 10 \oplus 10$ and $d_{sss} \to 8 \oplus 8$ channels. There are two possible $d^{--}_{sss} \to 10 \oplus 10$ channels, $\Sigma^{*-}\Xi^{*-}$ with the most promising decay chain being $d^{--}_{sss} \to \Sigma^{*-}\Xi^{*-} \to (\Lambda\pi^-)(\Xi^0\pi^-) \to (p\pi^-)(\pi^-)(\Lambda\pi^0) \to 2p\pi^0 4\pi^-$ which has a branching ratio of 41%. The other $10 \oplus 10$ channel is $\Omega^-\Delta^-$ with the most promising decay chain $d^{--}_{sss} \to \Omega^-\Delta^- \to (n\pi^-)(K^-\Lambda) \to npK^-2\pi^-$, which has branching ratio 44% .The only possible $d^{--}_{sss} \to 8 \oplus 8$ channel is $\Sigma^-\Xi^-$ with the decay chain $d^{--}_{sss} \to \Sigma^-\Xi^- \to (n\pi^-)(\Lambda\pi^-) \to np3\pi^-(Br = 64\%)$, where full measurement of Λ provide access to polarisation observables in d^{--}_{sss}.

As one can see in Fig. 15 the acceptance of the $d^{--}_{sss} \to \Omega^-\Delta^- \to (n\pi^-)(K^-\Lambda) \to npK^-2\pi^-$ reaction is very large even if all charged particles required to be measured in the FD. The acceptance is also very smooth, hence, no artificial bumps/deeps are expected to be produced by geometrical cuts.

In Fig. 16, one can see the angular distributions for the individual participants of the reaction $ed \to e'\Omega^-\Delta^- \to (n\pi^-)(K^-\Lambda) \to npK^-2\pi^-$, no d_{sss} formation condition was imposed. It is clear that the

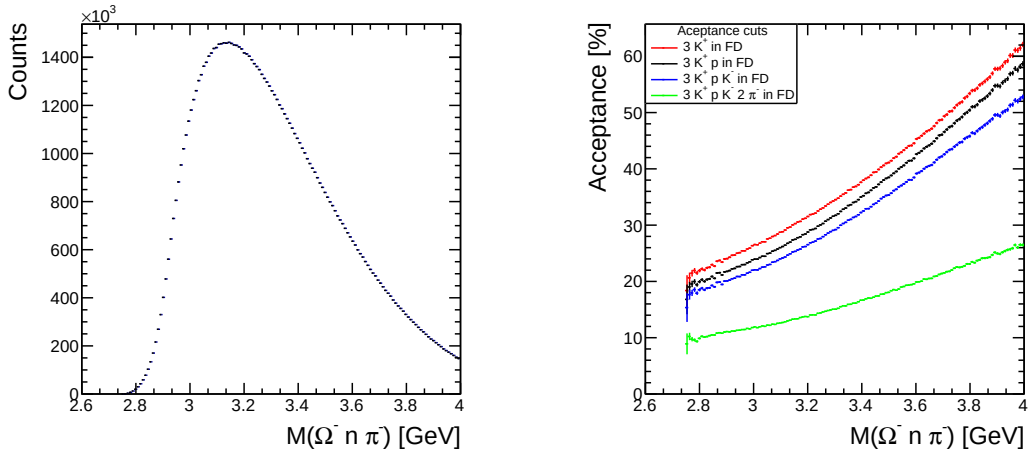

Figure 15: Simulated $\Omega\Delta$ invariant mass(left) and reaction acceptance as a function of $M_{\Omega\Delta}$ (right). Red line correspond to acceptance of the reaction if only $3K^+$ are measured in FD; black: $3K+$ and proton in FD; blue: $3K+$, proton and K^- in FD; green: $3K+$, proton, K^- and $2\pi^-$ in FD. (Phase space generation with $1/q^2$ weight for the virtual photon)

acceptance is large for all particles even if we limit ourselves for the FD detection only.

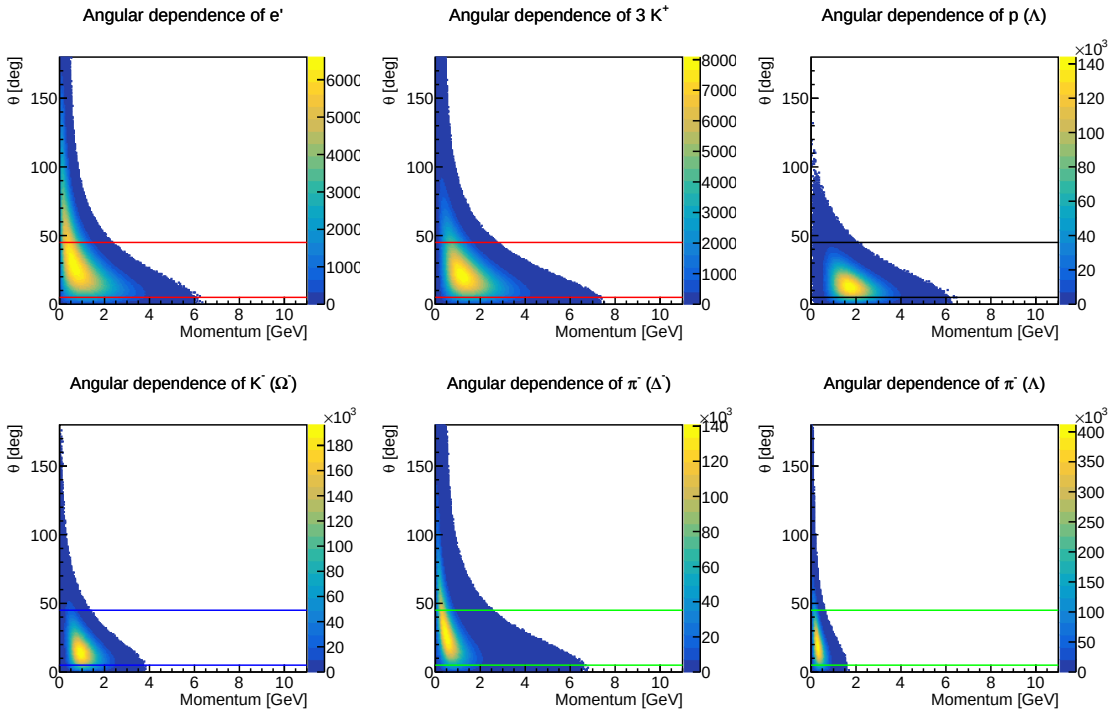

Figure 16: Simulated momentum-angular relations for the $\Omega\Delta$ electroproduction reaction. Horizontal lines highlight the FD acceptance range. (Phase space generation with $1/q^2$ weight for the virtual photon)

7 $\Omega\pi^-$ background for the d_{sss}-state

One should not expect any states in a strangeness $s = -3$ and charge $q = -2$ channel within the simple quark model picture. The minimum configuration which can cover such quantum numbers is the $\Omega\pi^-$ channel. There were several recent studies related to Ω and Ω_c interactions with an octet of mesons [28, 29]. One can expect dynamically generated resonances in some channels but not in $\Omega\pi^-$. It was shown already in Ref. [28] that a $\Omega\pi$ contact term is very repulsive. Unfortunately, no coupled channel analysis of an $\Omega\pi$ system had been performed so far, hence bumpy behaviour in an $\Omega\pi$ system due to coupled channels and/or threshold effects/cusp cannot be completely excluded.

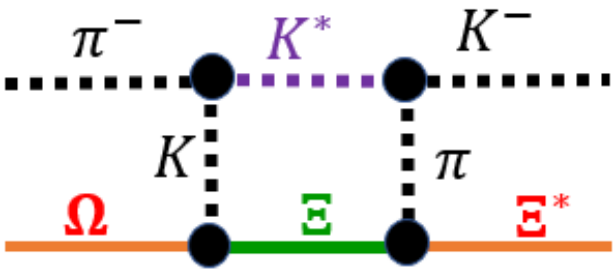

Figure 17: $\Omega\pi$ possible coupled channel graphs

One can identify three potentially dangerous regions near $\Omega\pi$, Ξ^*K and ΞK^* thresholds.

	$\Omega\pi$	Ξ^*K	ΞK^*
Threshold, MeV	1811	2024	2213
Width, MeV	0	10	51

It is interesting to note that the $\Omega\pi$ threshold lies even below the ΞK threshold (1815 MeV). We do not expect strong coupling between these two channels, however, a closeness of two thresholds 1811 MeV vs 1815 MeV might create some unusual behaviour. A study of this channel might provide important information about couple channel dynamics in the exotic triply strange system as well as supply information about d_{sss} background.

First evaluations were performed based on CLAS12 data rg-A data with the electron in Forward Detector. All 3 positive Kaons were selected in FD with tight $\Delta\beta - p$ cuts tuned on exclusive $\gamma^* p \to K^+\Lambda$ reaction. The missing mass of e^-3K^+, without sideband subtraction, shows a very small count rate, Fig. 18, proving a small background level for the d_{sss} production. Further increase in statistics might elucidate dynamics of an $\Omega\pi$ system. An absence of kaon mass sideband subtraction is clearly visible since all the background is concentrated in a kinematically forbidden subthreshold region. The specific topology studied is $ed- > e'd_sK^+$ and the d_s would decay as follows $d_s- > \Lambda n$

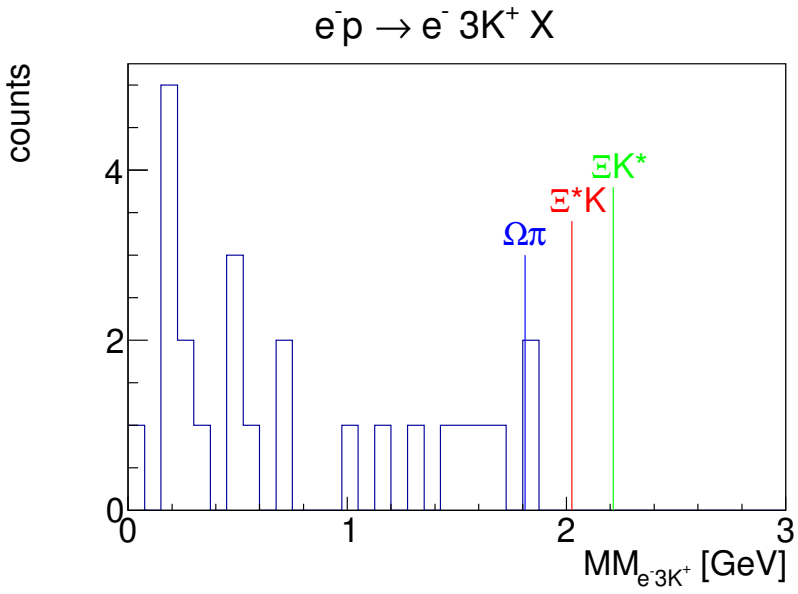

Figure 18: rg-A $\gamma^* p \to 3K^+X$ reaction study, $MM(e^-K^+K^+K^+)$. with appropriate thresholds shown as vertical lines.

8 Ongoing RGB Studies

According to requirement of the CAA committee we have performed several studies to check how well we can handle the RGB data to perform strangeness studies in general and dibaryon searches in particular.

8.1 RGB Feasibility

Since the fully exclusive reconstruction of the d_{sss} final state is challenging, we also performed some studies on the possibility of semi-inclusive analysis with $3K^+$ and a recoil electron being measured. As it was pointed out by the reviewers, the main issue would be a kaon misidentification. There are several reliable methods for how it can be treated safely. The one we used for the benchmark studies of the rg-A data with single and double kaon production is a sideband subtraction of a kaon mass plot, Fig. 19.

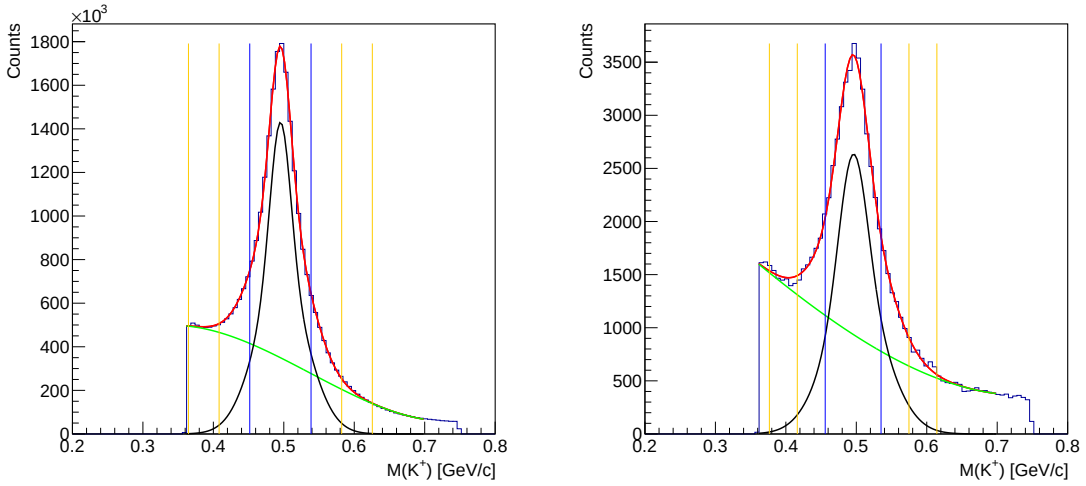

Figure 19: rg-A kaon mass plot distribution with particle mass calculated based on measured velocity (β) and particle momentum. Strangeness 1 (left) and strangeness 2 (right) [the first, fastest kaon out of the two]. Fitted curves showed peaked signal (black) from kaon as well as a smooth misidentification background production (green). For the sideband subtraction below, the signal region is between the two blue lines and sidebands between the two sets of yellow lines. (rg-A data from Spring 2019).

By defining signal and background sidebands as mean $\pm 3\sigma$ and mean $\pm 6\sigma$ to mean $\pm 9\sigma$ respectively for strangeness 1, one can make a $e'K^+$ missing mass plot, Fig. 20 (centre). Similarly one can produce a sideband subtracted $e'K^+K^+$ missing mass plot for a strangeness - 2 case, Fig. 21 (centre), using mean $\pm 2\sigma$ and mean $\pm 4\sigma$ to mean $\pm 6\sigma$ for signal and sidebands respectively.

Another background subtraction method was explored, hereafter referred to as continuous background subtraction, wherein the fit functions for the kaon's calculated mass is used to include the whole data set not just the mean +/- 2/3 σ. Using a 2D histogram of kaon mass and missing mass, the signal and background contributions are fit for the kaon's mass (same as sideband subtraction). Next, two projections of the missing mass are taken for every bin in the kaon mass, one for the 'signal' and one for the 'background' and scaled according to the scaling factors in Eq. 1,2. All the projections are added together for signal and background separately, then the background histogram is scaled so the integrals at low energies are equal between the background and signal histogram; this is done to make sure the lower energy background matches well and is removed properly. The resulting background histogram is subtracted from the signal histogram to get the final result.

$$\text{Signal scaling factor} = \frac{\text{Total function}}{\text{projection integral}} \tag{1}$$

$$\text{Background scaling factor} = \frac{\text{Background function - Signal function}}{\text{projection integral}} \tag{2}$$

Neither method is completely finalised, there is a small issue of over-subtraction in strangeness 1. However, both methods appear very effective in removing background without reducing the signal.

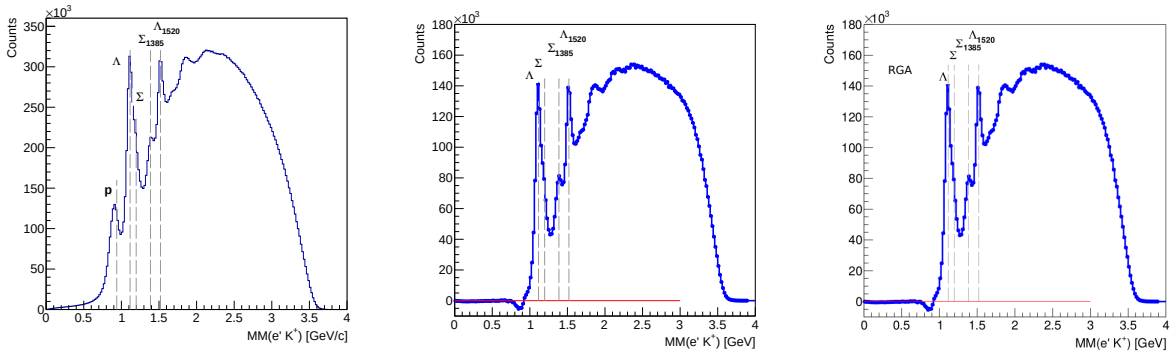

Figure 20: rg-A $e'K^+$ missing mass before background subtraction (left), with sideband subtraction (middle), and continuous background subtraction (right).(rg-A data from Spring 2019)

Fig. 20 (left) demonstrates $e'K^+$ missing mass prior to background subtraction. The misidentified pion background is noticeable as a subthreshold surplus of events. It gets completely eliminated by either of the background subtracting methods, Fig. 20(middle,right). All hyperons are nicely visible. The broad bump under the hyperon peaks does not originate from pion misidentification and/or event mixing. It comes from in-flight kaon production, Fig. 22(left).

We have performed similar studies for the strangeness 2 case.

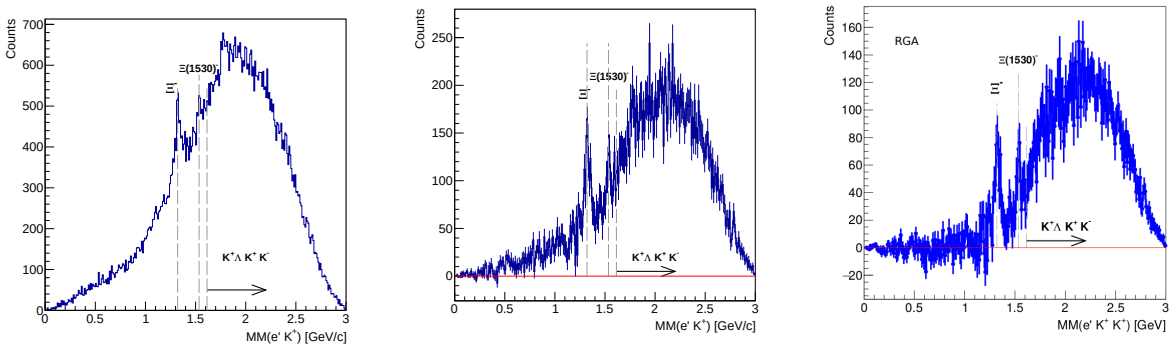

Figure 21: rg-A $e'K^+K^+$ missing mass before background subtraction (left), with sideband subtraction (middle), and continuous background subtraction (right).(rg-A data from Spring 2019)

Here the pion misidentification background gets even larger, but can be completely eliminated. Due to broadness of the kaon peak and narrow $\pm 4-6\sigma$ sidebands, the usual "sideband" subtracting technique does not make a full job. However, "continuous background subtraction", does the job pretty well. All subthreshold background gets completely eliminated, the first two cascades become clearly visible on top of nearly no background. The main background has a physical origin from kaon in-flight production, Fig. 22(right), and has very smooth behaviour.

These studies show clear potential for a $3K^+$ semi-inclusive analysis where comparison of distributions from proton and deuteron targets can help to elucidate the two-nucleon based $3K^+$ production processes.

The background subtraction was very effective for strangeness 1 and 2, suggesting strangeness 3 will also be promising. Currently, work is being performed on the background subtraction of strangeness 3 events.

Another very important question to address, is if we can treat RGA and RGB data in a similar manner. To investigate this point we have performed similar analysis on strangeness 1 and 2 data from RGA (Spring2019) and RGB (Spring2020) data with similar statistics. The results can be seen on Fig. 23 and Fig. 24.

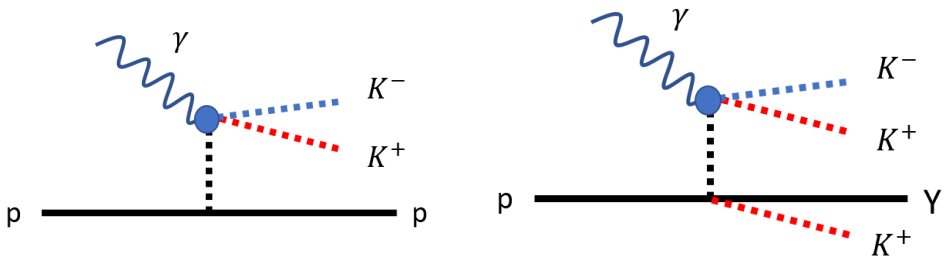

Figure 22: Diagrams of the typical kaon in-flight production backgrounds for single K^+ (left) and double-K^+ (right) production.

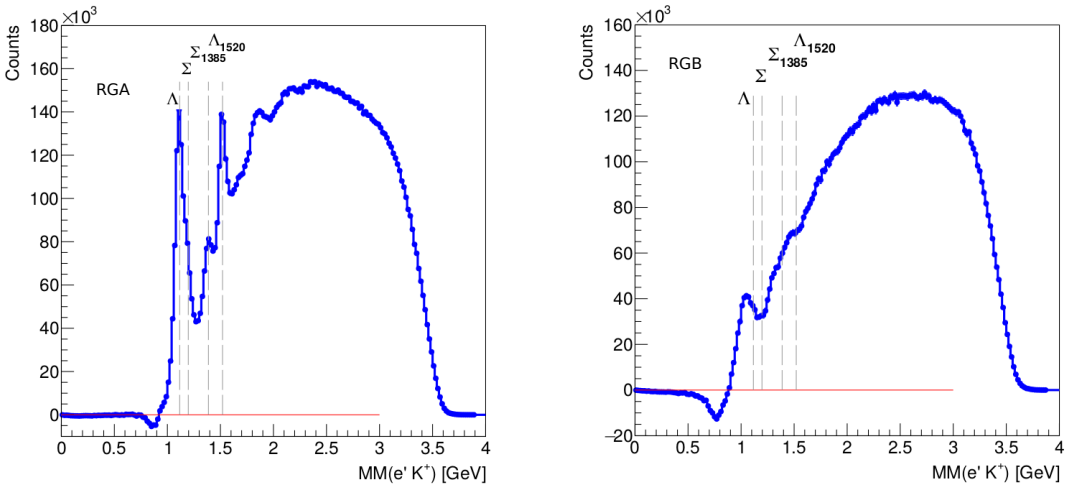

Figure 23: $e'K^+$ missing mass with continuous background subtraction based on kaon mass. RGA data (left) and RGB data (right). rg-A data from Spring 2019, rg-B data from Spring 2020

Both datasets exhibit very similar behaviour. The same continuous background subtraction techniques work pretty well. As expected, hyperon peaks in RGB data look smeared. The effect is two-folded: first of all, the existing calibrations of RGB are worse than RGA; secondly, the Fermi motion of a proton inside deuteron unavoidably smeared distributions while missing mass is calculated assuming the target was at rest.

The same effect is observed in strangeness 2 case. Very similar distributions in both datasets with somewhat smeared hyperons in the case of RGB.

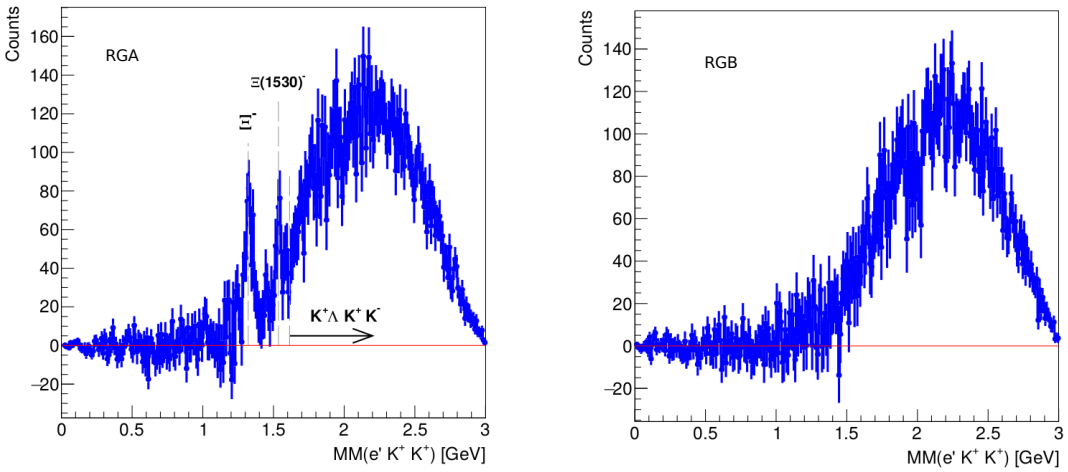

Figure 24: $e'K^+K^+$ missing mass with continuous background subtraction based on kaon mass. RGA data (left) and RGB data (right). rg-A data from Spring 2019, rg-B data from Spring 2020

8.2 Exploratory study of the d_s hexaquark production

While current calibration accuracy does not allow us to study d_s channels with K^0, we have to concentrate our efforts on exotic channels accompanied with charged kaons. As discussed in Section 4, the d_s can be formed with a K^+. Preliminary results from studies of one of these reactions are shown below. The specific reaction studied here is $ed \to e' d_s K^+$ where the d_s would decay to Λn and the Λ decays to $p\pi^-$. The main reasons for pursuing this channel are as follows. First, the balance of larger branching ratio for the smaller number of final state particles. Second, is the fact that from both the $d^*(2380) \to \vec{p}\vec{n}$ and from theory the Λ is expected to be 100% polarised at near 90° in case of d_s production. And since the Λ is self-polarising, this information is held in the angular distributions of the proton and π^-. This polarisation observable should be a lot more sensitive to a resonance behaviour compared to simple "bump hunting". As in the $d^*(2380)$ case, we do not expect to see a bump in $M_{\Lambda n}$ invariant mass from the Λn channel ($d^* \to pn$ analogue), but one might expect to see a rapid polarisation variation of the Λ in the case of the d_s resonance.

Below we show the results of analysis for the spring 2019 run of rg-B data. An initial skim of this data was preformed to select the $ed \to e' \Lambda n K^+$ channel. This was achieved by requiring at-least one electron, proton, π^- and K^+ (all in the forward detector). To clean the sample further, additional particle identification cut $|\chi^2| < 5$ was imposed. The results of the skim can be seen in Fig. 25, where we demonstrate the missing mass of all measured particles (left) and invariant mass of $p\pi^-$(right). Despite a very rough selection, one immediately sees the reaction of interest. The missing mass of all measured particles Fig. 25(left) demonstrates a rather narrow peak at the position of the unmeasured neutron, highlighted by a dashed red line. On the Fig. 25(right) one can see a small peak corresponding to the Λ with a nominal mass also highlighted by a red dashed line accompanied by the smooth background and a broad peak at 1232 MeV, originating from a Δ resonance which appeared here due to $\pi^+ \to K^+$ misidentification.

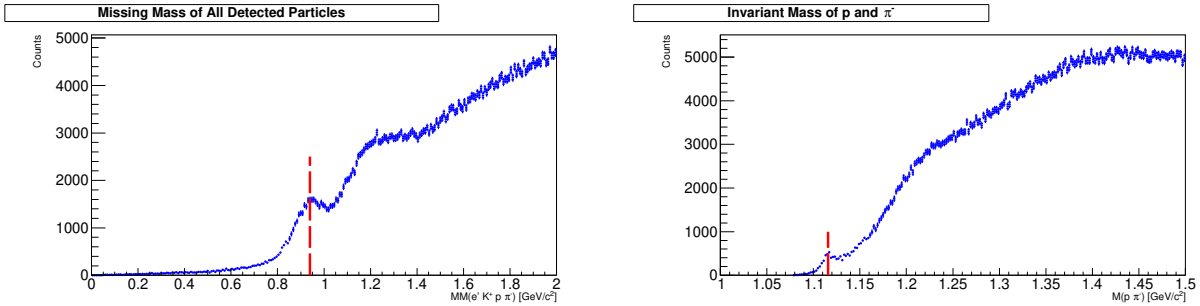

Figure 25: On the left is the missing mass of the scattered electron, K^+, proton and π^- this to search for the undetected neutron. On the right is the invariant mass of the proton and π^- looking for the Λ. The red dashed line in both represent the nominal masses for each baryon.

After skimming, we have applied a few more cuts to clean up the reaction of interest. First, we impose a cut on the missing neutron Fig. 25(left), by fitting the peak with a Gaussian signal and a polynomial background and only accepting events within $\pm$ 3σ. Then we cross-check the p π^- invariant mass Fig. 26. The Λ peak close to the threshold becomes a lot more pronounced and the uncorrelated background is reduced considerably. A nice, broad second peak can still be seen at about 1.232 GeV from the Δ baryon. It is also clear that the leakage of both the Δ and the uncorrelated events under the Λ peak is minimal.

Finally, we cleaned up our sample by selecting Λ events with $M_{p\pi^-} < 1.14\ GeV/c^2$ invariant mass cut. At this point one can consider our sample to be relatively clean from backgrounds and we can start with investigation of underlying physics. The effect of reaction selection can be also seen on Fig. 27, where the left side show the momentum of missing neutron before(left) and after(right) cuts. From a structureless distribution we got something reasonable, dominated by quasi-free Λ production on proton accompanied with a neutron spectator. A slightly wide missing neutron momentum distribution originates from yet non-perfect RG-B calibration. For the d_s studies only events with high neutron momentum are of interest, since only for those event neutron acts as an active member of the reaction, rather than passive quasi-free observer. A proper event-separation technique utilising polarisation observables to disentangle Quasi-Free/Active events were

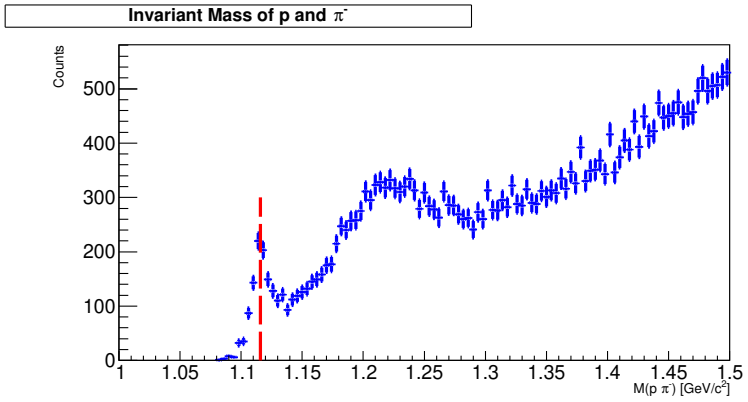

Figure 26: Invariant mass of the proton and π^- after a mean $\pm$ 3 sigma cut on the missing neutron peak in Fig 25. This is again plotted to search for the Λ and the red dashed line is the nominal mass.

recently developed by N. Zachariou (see Ref. [30] and Ref. [31]). We plan to use it in our studies as well.

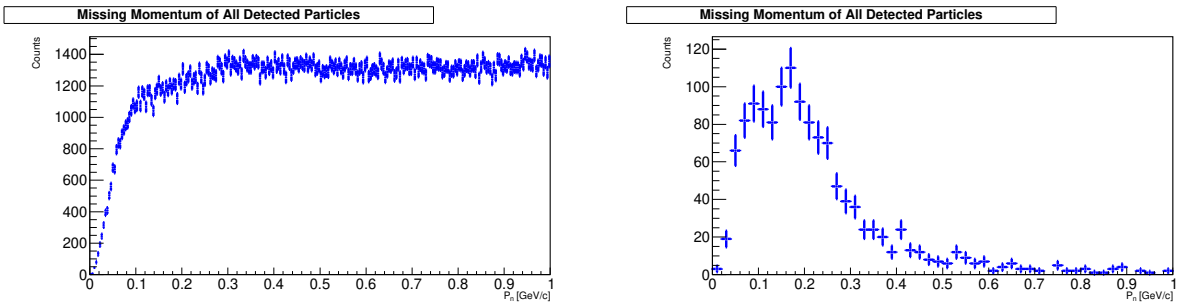

Figure 27: Both plots here show the momentum of the missing neutron. On the left is before any selection cuts. On the right is after cutting on the missing neutron peak with mean $\pm$ 3 sigma and invariant mass of proton and π^- less than 1.14 GeV.

As a next step we will extract the polarisation of the Λ baryon as a function of Λn invariant mass and Λ angle (in the d_s rest frame). The extraction of this quantity requires GEMC simulations to correct those distributions for acceptance and efficiency effects of CLAS detector. From those studies we can directly get the polarisation of Λ due to its self analysing nature(note that the Λ self-analysing coefficient was recently reevaluated and a new PDG value gets larger, simplifying this kind of analysis [32]). As a final goal we want to get Λ polarisation for a 90° deg angle as a function of d_s mass (equal to missing mass of $e'K^+$) to perform similar analysis as in the case of the $d^* \rightarrow pn$ reaction [26], we hope to see a peak corresponding to a d_s production on top of slowly varying conventional background. One also might see a cusp behaviour at the ΣN threshold due to $\Lambda N <-> \Sigma N$ coupled channels [33].

References

[1] R. Aaij *et al.*, Phys. Rev. Lett. **112**, 222002, (2014)

[2] R. Aaij *et al.*, Phys. Rev. Lett. **122**, 222001, (2019)

[3] M. Bashkanov *et al.*, Phys. Rev. Lett. **102**, 052301 (2009).

[4] P. Adlarson *et al.*, Phys. Rev. Lett. **106**, 242302 (2011).

[5] P. Adlarson *et al.*, Phys. Rev. Lett. **112**, 202301 (2014).

[6] P. Adlarson *et al.*, Phys. Lett. B **721**, 229, (2013)

[7] P. Adlarson *et al.*, Phys. Rev. C **88**, 055208 (2013).

[8] P. Adlarson *et al.*, Phys. Lett. B **743**, 325 (2015).

[9] P. Adlarson *et al.*, Eur. Phys. J. A **52**, 147 (2016).

[10] P. Adlarson *et al.*, Phys. Rev. C **90**, 035204 (2014).

[11] M. Bashkanov, H. Clement, T. Skorodko, Eur. Phys. J. A **51** (2015) 7, 87.

[12] Fei Huang, Peng Nian Shen, Yu Bing Dong, Zong Ye Zhang, Sci. China Phys. Mech. Astron. **59**, 622002 (2016).

[13] M. Bashkanov, Stanley J. Brodsky, H. Clement Phys.Lett. B**727**, (2013), 438-442

[14] I. Vidaña Hyperon puzzle, Proceedings of the Royal Society A474, 20180145

[15] I. Vidaña, M. Bashkanov, D.P. Watts, A. Pastore, Phys. Lett. B **781**, 112-116, (2018).

[16] A. Mantziris, I. Vidaña, M. Bashkanov, D.P. Watts, A. Pastore, A.M. Romero, arXiv:2002.06571.

[17] Ben Margalit and Brian D. Metzger, Astrophys.J. 850, no.2, L19 (2017)

[18] P. Demorest, T. Pennucci, S. Ransom, M. Roberts, J. Hessels, Nature **467**, 1081 (2010).

[19] J. Antoniadis *e*t al., Science **340** 6131(2013).

[20] E.Annala *et al.*, arXiv:1711.02644v1

[21] M. Bashkanov and D.P. Watts, J. Phys G **47**, no.3, 03LT01, (2020)

[22] M. Guenther, Master Thesis, University of Basel (2015); PoS (Hadron2017) 051.

[23] T. Ishikawa *et al.*, Phys. Lett. B **772**, 398, (2017).

[24] M. Bashkanov and D.P. Watts, Phys. Rev. C **100**, no.1, 012201, (2019)

[25] M. Bashkanov *et al.*, Phys. Lett. B**789**, 7, (2019).

[26] M. Bashkanov *et al.*, , Phys. Rev. Lett. **124**, 132001, (2020)

[27] T. Ishikawa *et al.*, Phys. Lett. B **789**, 413, (2019).

[28] E.E. Kolomeitsev, M.F.M. Lutz, Phys. Lett. **B585**, (2004), 243

[29] M. Döring, E. Oset, D. Strottman, Phys. Lett. **B639**, (2006), 59

[30] N. Zachariou, E. Munever *et al.*, arXiv:2106.13957v1

[31] S. Ayub, Masters thesis, Uni. York 2022

[32] P.A. Zyla *et al.* (Particle Data Group), Prog. Theor. Exp. Phys. 2020

[33] S. Jowzaee, E. Borodina *et al.*, Eur. Phys. J. A **52**, 7 (2016).